Journal of Coastal Research	16	3	840–852	West Palm Beach, Florida	Summer 2000

Tidal Motion in a Complex Inlet and Bay System, Ponce de Leon Inlet, Florida

Adele Militello† and Gary A. Zarillo‡

† USAE Waterways Experiment Station, Coastal and Hydraulics Laboratory, 3909 Halls Ferry Road, Vicksburg, MS 39180, U.S.A.

‡ Division of Marine and Environmental Systems, Florida Institute of Technology, 150 W. University Blvd., Melbourne, FL 32901, U.S.A.

ABSTRACT

MILITELLO, A. and ZARILLO, G.A., 2000. Tidal motion in a complex inlet and bay system, Ponce de Leon Inlet, Florida. *Journal of Coastal Research,* 16(3), 840–852. West Palm Beach (Florida), ISSN 0749-0208.

Tidal motion and inlet processes were investigated in Ponce de Leon (Ponce) Inlet, Florida and its bay channels through a 10-week data-collection campaign and two-dimensional numerical simulation modeling. Water level and current were measured at six locations spanning the ebb shoal, inlet, and bay channels. Measurements revealed that the inlet was flood dominated during the data-collection period. The flood dominance may have been enhanced by a net influx of water during the measurement period, which was captured at two measurement stations in the bay channels located 5 km away from the inlet.

Scour, erosion, and sedimentation are problems faced at Ponce Inlet, and calculations suggest tide-related circulation patterns contribute to problematic hot spots. Scour along the north jetty may be most active on the ebb tide, when the strongest flows oriented parallel to the jetty are present. Erosion on the north interior spit owes to a bend in the inlet that forces the strong flood current to impinge on the spit shoreline. Progradation of the south spit into the inlet is a product of the curvature of the spit that creates a region of relatively weak current in the southern portion of the inlet. Deposition may therefore occur on both flood and ebb tidal cycles.

Tidal attenuation was calculated along a 7 km transect from the ebb shoal, through the inlet, and south along the Indian River North. Attenuation of the M_2 tide (water level) was estimated to be 1.1 cm/km along the unimpeded reach of the transect extending south from the ebb shoal to just north of a bridge. At the bridge, the attenuation was increased to 55 cm/km, a decay that is 50 times greater than in the unimpeded channel. The bridge was found to contribute to 56% of the tidal-amplitude reduction between the ebb shoal and the bridge.

ADDITIONAL INDEX WORDS: *Tidal inlet, inlet hydraulics, tidal attenuation, flood dominance, circulation modeling, tide measurement.*

INTRODUCTION

Tidal inlets and the associated bays behind them are subject to a wide range of driving forces that create unique hydrodynamic conditions for each inlet and bay system according to its geometry and bottom topography. Understanding of sedimentation and scour patterns within inlets and navigation channels can be improved by resolving circulation patterns controlled by the acting physical processes. For instance, in the direct vicinity of an inlet, tidal motion dominates the flow. However, in distant reaches of a bay, other processes such as river flow or wind may dominate. The presence of hydraulics structures, such as bridges, can disrupt the pattern of tidal flow, modifying the tidal amplitude and currents. This study identifies the circulation patterns and investigates tidal propagation and attenuation in a complex inlet and bay system with hydraulic structures.

Tidal wave propagation is accompanied by attenuation. Bottom friction works to both modify the spectra of the water motion and reduce the tidal amplitude with distance into an estuary or bay. Attenuation is strong in systems containing significant tidal flats, shoals, and shallow water. Sediment transport is linked to tidal attenuation by two general means: 1) damping of the tide alters the strength of the current, which induces scour and deposition, and 2) as the tide attenuates with distance from an inlet, other processes such as wind or river inflow can become dominant, resulting in circulation patterns that may be different from those produced by the tide. Additionally, modification of the bottom topography influences the tidal propagation. Thus, a feedback mechanism can occur between the tidal hydrodynamics and sediment transport through bottom topography change.

Bridges can significantly modify tidal propagation through a channel or bay because these structures behave as point sources of tidal-amplitude reduction. The upstream side of a bridge can possess significantly smaller tidal amplitude as compared to the downstream side. Thus, bridges can define the boundaries between hydraulic regimes, or compartments, that have different circulation patterns (SURAK, 1994, BROWN *et al.,* 1995). However, little work has been conducted on the resistance that bridges impose on tidal flows, and

98266 received 30 November 1998; accepted in revision 15 May 1999.

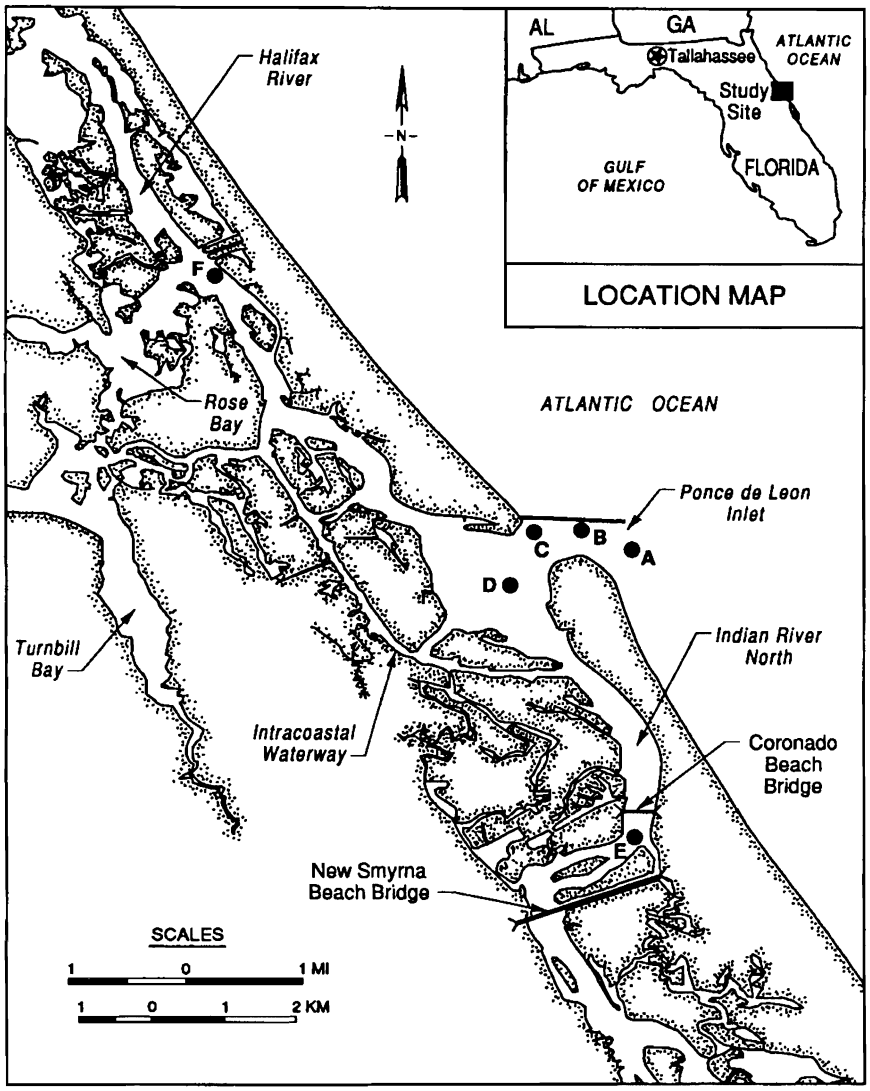

Figure 1. Location map of the Ponce de Leon Inlet study site. Measurement station locations are shown as filled circles.

MEHTA (1996) has identified this topic as having high priority for inlet-related research.

Tidal motion at Ponce de Leon (Ponce) Inlet, Florida and its adjacent bay channels is examined here by field measurements and application of a two-dimensional, depth-integrated hydrodynamic numerical model. Circulation patterns in the inlet are identified and discussed in relation to localized scour and deposition. Attenuation of the M_2 tidal constituent is investigated along a reach of the inlet and bay system and quantified in terms of an amplitude reduction per unit length of channel. The change in tidal amplitude at a bridge is also included as part of this investigation of the flow at a complex inlet and back-bay system.

STUDY SITE

Ponce Inlet is located on the east coast of Florida and lies approximately 92 km north of Canaveral Harbor (Figure 1). The area of study includes the inlet, ebb shoal, and back bay and associated channels. Stabilization of the inlet was initiated in 1968 and completed in 1971. Two jetties were constructed and as part of a sand bypassing system, the north jetty was constructed with a weir section. The weir did not function as anticipated, and scour occurred in the northern inlet throat while the south spit migrated into the inlet (PARTHENAIDES and PURPURA, 1972; PURPURA, 1977; JONES and MEHTA, 1978). The weir was closed in 1984, but scour at the north jetty and encroachment of the south spit into the inlet has continued (TAYLOR *et al.*, 1996, HARKINS *et al.*, 1997). Erosion of the north interior spit, west of the north jetty, increased upon weir closure (HARKINS *et al.*, 1997). Presently, the south jetty is almost entirely buried by sand.

Ponce Inlet is hydraulically linked northward to the Halifax River and southward to the Mosquito Lagoon via the Indian River North. In this area of the Central Florida Coast,

Figure 2. Aerial photograph taken March 21, 1996, showing the flood shoal west of Ponce de Leon Inlet. Rockhouse Creek splits the shoal into two lobes.

the mean tidal range in the ocean is approximately 1 m, and the mean spring range reaches 1.3 m. The tide is semi-diurnal, with the M_2 amplitude dominating other constituents by an order of magnitude or more. The barrier island systems to the north of Cape Canaveral typically possess a narrow and low-profile structure, well-developed flood shoals, and ebb shoals of smaller volume that are largely submerged (HAYES, 1979, ZARILLO *et al.*, 1982). Although the bay directly west of the inlet throat retains its natural configuration, a navigation channel was dredged west of the bay in the 1950's as part of the Intracoastal Waterway (IWW) system (Figure 1). The IWW traverses the length of the study site and is the major channel within the Halifax River/Mosquito Lagoon complex away from the inlet. Design dimensions of the IWW are 90 m width and 3.7 m depth. The confluence of the IWW and the Halifax River lies 3.5 km north of the inlet, and the IWW joins the Indian River North 2 km south of the inlet.

West of the inlet, the flood shoal occupies a significant amount of the bay area, as shown in Figure 2. Rockhouse creek is a tidal channel that bifurcates the shoal and provides direct exchange between the inlet and the IWW. The flood

shoal is exposed during much of the tidal cycle so that flow is commonly restricted to the main channel and Rockhouse Creek. Other natural features in the area include Rose Bay and Turnbill Bay and numerous small channels that provide water exchange for marsh and mangrove habitats of the area. These channels and bays act as storage for water flowing into and out of the Ponce Inlet system.

The Coronado Beach Bridge is one of eight bridges that span the Halifax River/Mosquito Lagoon complex. This bridge crosses the Indian River North approximately 4 km south of Ponce Inlet and is the closest bridge to the inlet. The circulation model is applied to estimate the tidal amplitude attenuation at the bridge.

MEASUREMENTS

Synoptic measurements of water level and current velocity were collected at six locations in the Ponce Inlet system (Figure 1) from August 21 through November 1, 1997 (ZARILLO and MILITELLO, 1999). The measurement strategy was aimed at collecting data for calibration of the circulation model and a wave-propagation model (SMITH and SMITH, 1999) and to augment long-term data collection at the site (KING *et al.*, 1999). Station A was located on the ebb shoal, whereas Stations B and C were located in the main inlet conveyance channel. Station D was located west of the main inlet channel and east of the flood shoal. Station E was located approximately 5 km south of the inlet in the Indian River North (0.8 km south of the Coronado Beach Bridge), and Station F was located on the Halifax River approximately 5 km north of the inlet. Stations D, E, and F were leveled with respect to the National Geodetic Vertical Datum (NGVD).

Instrument packages for fixed-station monitoring each consisted of a 2-axis Marsh-McBirney electromagnetic current meter combined with a high-resolution pressure transducer (puv-type sensors). Current velocity and water-level measurements were calculated from a 1-min average of samples taken at 1 Hz. The sampling interval was one hour. All sensors were calibrated before and after field deployment.

Bottom topography at the study site was acquired by the SHOALS lidar system (LILLYCROP *et al.*, 1996) during September and October 1996 surveys. Data were collected at 4 m $\times$ 4 m horizontal resolution. The area of survey coverage included the inlet, ebb shoal, nearshore zone north and south of the inlet, and limited reaches of the Halifax River and Indian River North. Maximum depth of the survey was 9 m, and elevations were referenced to the NGVD. The dense SHOALS data were reduced to 7 m $\times$ 7 m resolution by application of the minimum curvature gridding method. The processed bottom topography was output to a rectangular grid.

Comparisons of current speed, current direction, and water-elevation time series were made among the six stations to determine if water level, tidal phase, tidal amplitude, and current magnitude were consistent with respect to station position and inlet geometry. This review resulted in the elimination of short segments of data from Stations A and F that may have been contaminated by low battery power or electronic noise.

National Ocean Service (NOS) standard harmonic analysis methods were applied to all water-level data from stations having continuous records of 29 days or longer to calculate tidal constituents. Where possible, harmonic analysis of overlapping 29-day segments of water-level data were conducted, and the results were vector averaged to provide a more stable estimate of tidal constituents. Shortened time series at Stations A and F allowed harmonic analysis on a single 29-day record in each case.

CIRCULATION MODEL SETUP AND CALIBRATION

Hydrodynamic modeling of the study site was conducted by application of the two-dimensional, depth-integrated, finite-element model ADCIRC (LUETTICH *et al.*, 1992). The numerical grid encompassed Florida's east coast and contains the entire Halifax River and Mosquito Lagoon complex within the computational domain (Figure 3). Details of the grid in the inlet and limited back-bay area are shown in Figure 4. High resolution was specified in the inlet and back bay regions to calculate water level and current over the complex bottom topography. The grid was constructed using National Oceanic and Atmospheric Administration bottom topography in the Atlantic Ocean. SHOALS data were applied to define the bottom topography in the vicinity of Ponce Inlet, including the inlet, ebb shoal, and limited back-bay channels. Flood-shoal elevations were estimated from aerial photographs. In the remaining interior regions, bottom elevations were applied from NOS charts. All bottom topographic data were converted to Mean Sea Level (MSL). Figure 5 shows the bottom topography specified in the model in the vicinity of the inlet. The inlet gorge and ebb and flood shoals are well defined by the bottom topographic data.

The model was forced at its ocean boundaries with four semi-diurnal tidal constituents M_2, N_2, K_2, S_2, and four diurnal constituents K_1, P_1, Q_1, and O_1 developed from a previous ADCIRC modeling effort (WESTERINK *et al.*, 1993). Simulations were conducted with the finite-amplitude and advective terms included in the computations. Wind fields were obtained from the National Center for Environmental Prediction and applied over the model domain. Wind information was specified at a spatial resolution of 0.25 deg and temporal resolution of 6 hr. Resolution of the wind field was sufficient for simulating large-scale meteorological forcing, but not mesoscale motions such as sea breeze. Thus, water motion induced by mesoscale wind processes was not simulated. The specified time interval for the simulation was from August 22, 1997 (Julian Day (JD) 234) to October 24, 1997 (JD 297). During the simulation period, no storms passed through the study area.

The Coronado Beach Bridge was represented in the computational grid by modification of the bottom topography. At the bridge site, depths were reduced over much of the width of the Indian River North, leaving a narrow region of channelized flow. The depths were adjusted until the calculated M_2 amplitude at Station E was close to that of the measurements.

Tidal constituents contained in the database from which

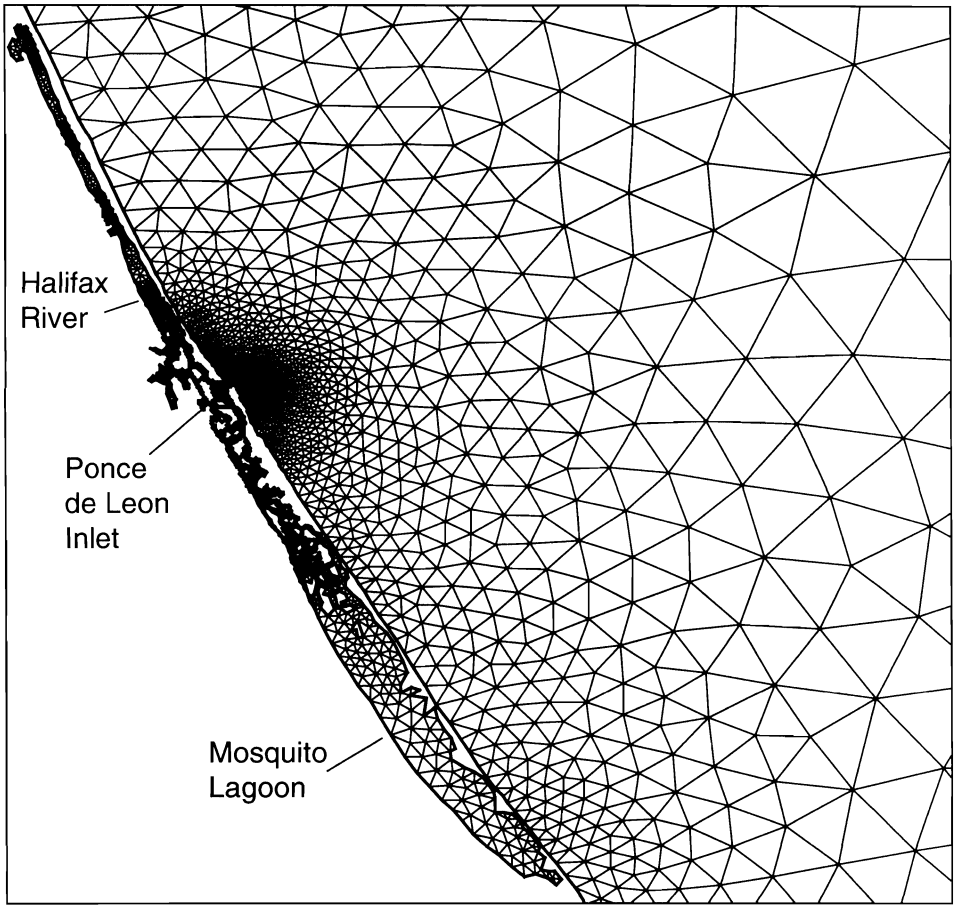

Figure 3. Regional view of finite-element grid showing Halifax River and Mosquito Lagoon complex.

the model ocean forcings were extracted are overpredicted in the northern region of the grid applied for this study (WESTERINK *et al.*, 1993). Calibration of the model was conducted by reduction of tidal amplitudes at the ocean boundary until calculated water levels were in agreement with measurements. Phases at the ocean boundaries were not modified. A spatially-constant drag coefficient was specified over the model domain and not modified during the calibration process.

Representative plots of water level from each of the six gauge locations are shown in Figure 6. Measured and calculated water levels are presented for comparison. Time series for Stations B, C, D, and E are presented for August 25, 1997 (JD 237) through September 1, 1997 (JD 244). Because of equipment problems at Stations A and F, the time series for those stations are presented for different dates than Stations B, C, D, and E. Time series for Stations A and F are shown for October 13, 1997 (JD 286) through October 20, 1997 (JD 293). Calculated water levels generally compare well to measurements. Station A shows the largest discrepancy, with the model consistently underpredicting the tidal peaks and troughs by 2 to 4 cm. The source of this underprediction is thought to be inaccurate calculation of shoaling of the tidal wave over the ebb shoal. Bathymetry data applied in the model for the ebb shoal were collected approximately one year before the simulation time. Because of the dynamic nature of the ebb shoal, sand movement may have locally modified the bottom between 1996 and 1997, which would correspondingly change the tidal shoaling properties in this area.

M_2 water-level amplitude and phase calculated by standard NOS harmonic analysis are given in Table 1 for measurements and model output. Within the inlet and at Station E, the difference in M_2 amplitude is 5 cm or less. The 9-cm amplitude difference at Station A may owe to inaccuracies in representation of the ebb shoal bottom topography, insufficient resolution over the shoal, or non-tidal processes active in the area that were not included in the circulation model. The 8-cm difference at Station F most likely owes to the presence of shoals in the Halifax River that are not represented in the model (detailed and recent bottom topographic data were not available away from the inlet). The difference in phase between the measurements and model calculations is typically about 30 deg, or approximately 1 hr for an M_2 tide. Minimum phase difference is 6 deg (0.2 hr) at Station E and maximum phase difference is 40 deg (1.4 hr) at Station F.

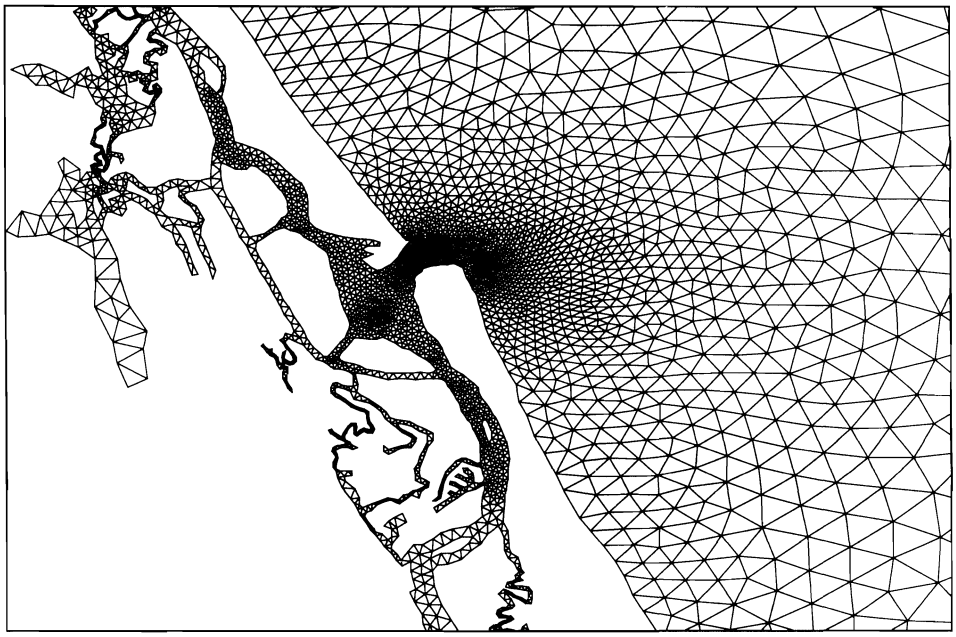

Figure 4. Detail of computational finite-element grid within the study area.

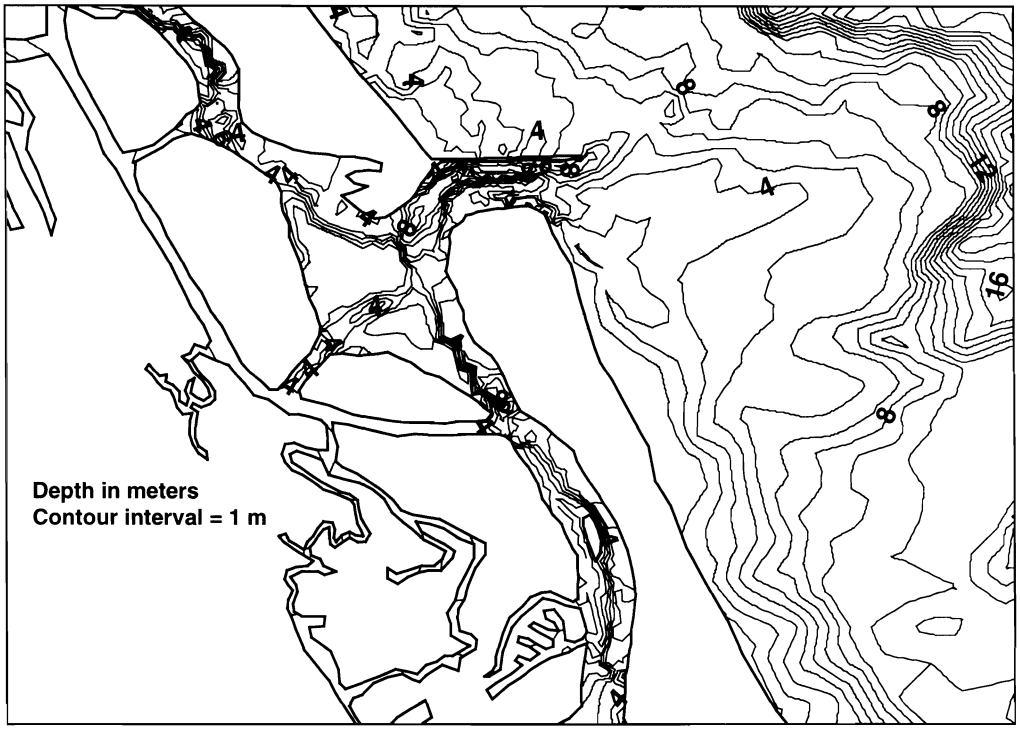

Figure 5. Bottom topography for the study area, relative to MSL.

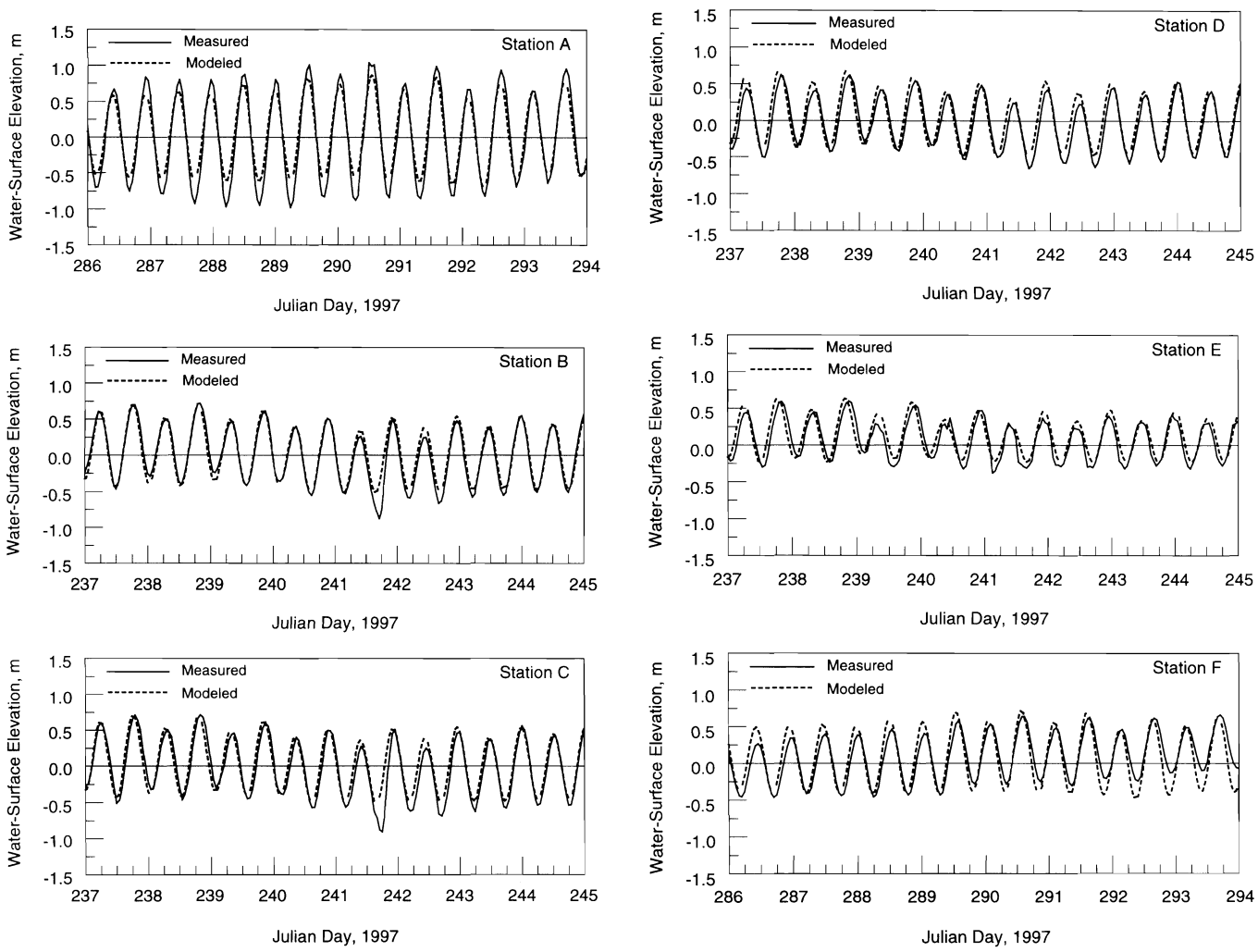

Figure 6. Representative measured and calculated water level (MSL) at instrument locations.

Phase errors may also be caused by inaccuracies in the bottom topography.

Measurements at Stations A, B, and C show flow dominance along the E–W alignment, owing to the orientation of the inlet. Comparison of measured and calculated E–W current speed at these three stations is shown in Figure 7. Positive values indicate flow toward the east. Calculated E–W current speed is underpredicted at Station A, particularly on flood flow. Error in the calculations may owe to the same sources as discussed for water-level calculations at Station A. Another source of error is comparison of velocity from a point current meter to a depth-integrated calculation. A significant difference in the tidal phase is evident between the measurements and calculated current. Because this phase error is greater at Station A as compared to Stations B and C, the increased error is thought to be caused by localized circulation that may not be well represented by the model. The E–W current calculated at Station B compares well to measurements. Generally, the current is over-predicted mainly during ebb tide. Contributing factors to the error at Station B are general over-prediction of the current, difference between measured and calculated tidal phase, and inexact replication of tidal asymmetry. At Station C, the E–W current matches well for ebb tide, but underpredicts significantly on flood tide. The following section includes discussion of a flood bias of the current present in the measurements that persisted for the

Table 1. *Comparison of measured and modeled M_2 tidal constituents at gauge locations.*

	Measured		Modeled	
Station	Amplitude, cm	Phase, deg	Amplitude, cm	Phase, deg
A	59	102	50	69
B	51	91	49	70
C	53	105	48	71
D	45	100	47	72
E	30	90	33	84
F	31	123	39	83

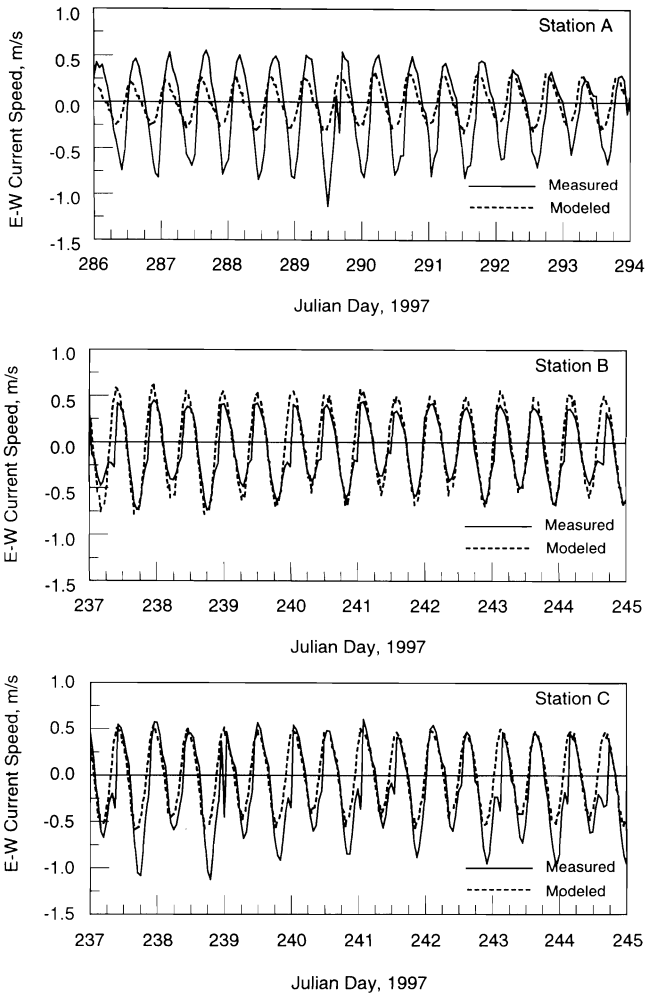

Figure 7. Representative measured and calculated E–W current speed at Stations A, B, and C. Positive values indicate flow toward the east.

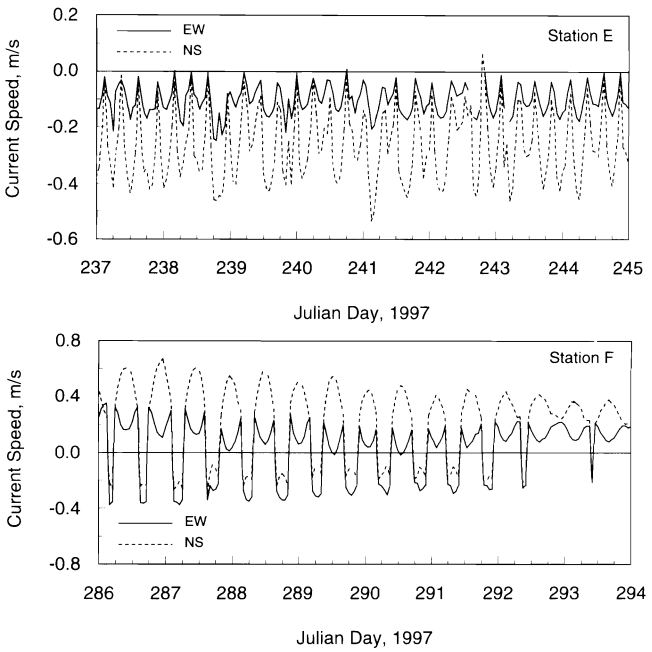

Figure 8. Representative measured current at Stations E and F. EW and NS denote flow parallel to the east-west and north-south axes, respectively. Positive values indicate flow toward the east and north.

duration of the data record. This bias was not simulated by the model and contributes to error in calculation of the current.

INLET CURRENTS AND CIRCULATION PATTERNS

Station A was located in a region of expanding and contracting flow as water moves out of and into the inlet and has currents that typically peak at approximately 0.5 m/s. Currents at Station B are stronger than at Station A, owing to Station B being located further into the inlet throat. Peak currents at Stations B are approximately 0.8 m/s and those at Station C exceed 1 m/s. Previous measurements within the inlet throat have shown that the peak current is approximately 1 m/s (TAYLOR *et al.,* 1996, KING *et al.,* 1998) and the present measurements agree with those collected in the past. A maximum current speed of approximately 1 m/s is required to maintain an inlet (O'BRIEN, 1969), and speeds in Ponce Inlet are sufficient for maintaining the inlet. Stations A, B, and C have stronger flood tidal currents than ebb current with the duration of the ebb portion of the tidal cycle exceeding that of the flood. These properties indicate that the inlet was flood dominated during the period of measurement.

Representative measured currents at Stations E and F are shown in Fig. 8. The current at Station E flowed toward the southwest throughout the duration of the data collection. This flow direction is along the principal axis of the Indian River North. The tidal flow is manifested as a strengthening of the southwest flow on flood tide and reduction of the flow to near zero at ebb tide. Peak flood current was typically about 0.5 m/s. Because the flow was directed upstream for the entire length of the record, there was a net influx of water into the Indian River Lagoon North and Mosquito Lagoon system.

Station F exhibited strongly asymmetric current motion with respect to flood and ebb tidal currents (Figure 8). Peak flood current was stronger and longer in duration than peak ebb current, and directed toward the northeast. The gauge was located in a section of the Halifax River that trends northwest and southeast, and where flow into and out of Rose Bay meets the Halifax River. The easterly flow component during flood tide and the westerly component during ebb tide may owe to a localized circulation resulting from the confluence of Rose Bay and the Halifax River. Reduction in the east-west flow component magnitude during peak flood represents turning of the current. Similar to the current record at Station E, the flow is largely directed upstream, indicating a net inflow of water into the Halifax River during the measurement period.

The process controlling the net influx of water at Stations

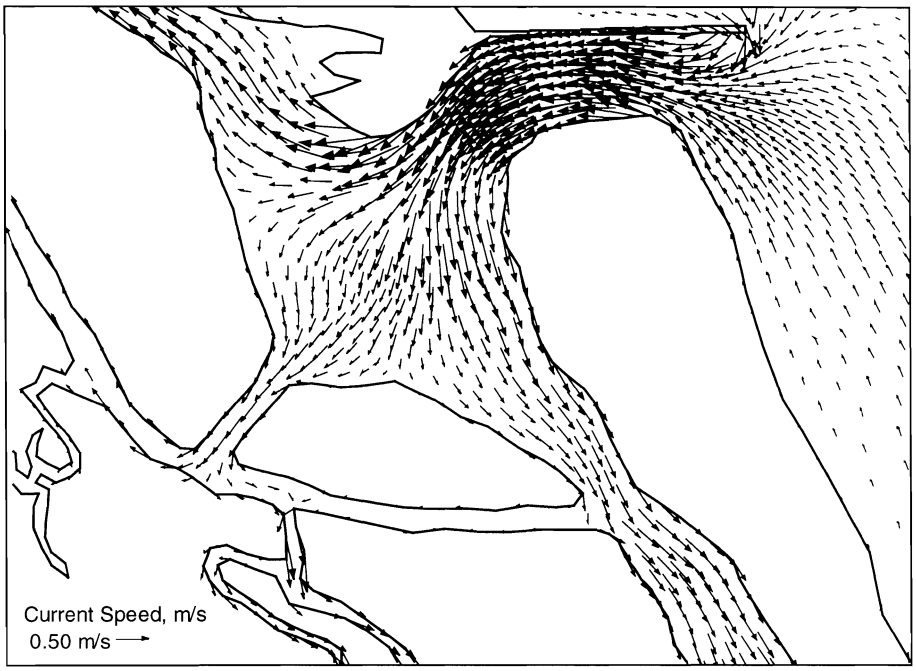

Figure 9. Flood tide circulation at Ponce Inlet. Current speed is indicated by vector length. An area with no vectors can represent either exposure of the bottom or weak current.

E and F was not investigated or modeled in this study. Calculated currents do not contain this long-period bias in flow direction because only the diurnal and semi-diurnal tidal constituents and large-scale wind fields were applied as forcing. Factors that may contribute to the net flow bias include a pressure gradient between the coastal ocean and back bays (such as induced by seasonal change in sea level or migration of the Gulf Stream), evaporation, and transport of water through canals located at the terminal ends of the Halifax River and Mosquito Lagoon. The duration of the influx is unknown, but it persisted through the measurement period.

Representative flood and ebb circulation patterns are shown in Figures 9 and 10, respectively. On flood tide (Figure 9), the strongest current is located within the inlet throat and the northern inlet exit (where the bay meets the inlet). Peak currents in the throat are approximately 1 m/s. Flood currents exiting the inlet are largely deflected by the flood shoal and travel north and south along the Halifax River and Indian River North channels, respectively. Currents are weak over the flood shoal, as expected. During the ebb portion of the tidal cycle (Figure 10), the strongest currents (1 m/s) are located within the inlet throat. Examination of Figure 10 reveals stronger currents on the eastern half of the inlet, adjacent to the north jetty, as compared to the western half. This pattern may indicate the flow structure responsible for scour along the eastern half of the north jetty. Currents entering the inlet from the Halifax River are also strong, approaching 1 m/s.

The flood shoal at Ponce Inlet is large and regularly inundated and exposed with tidal changes in water level. Flooding and drying is represented in the hydrodynamic model by turning elements on and off based on surrounding water level and current speed criteria. This capability allows for time-varying inundation and exposure of the shoal bottom in response to water-level changes. If the flood shoal were represented unrealistically by always keeping a section dry or keeping the shoal inundated at all times, computed water level and current patterns would not be realistic and could result in incorrect representation of tidal asymmetry. Typical current patterns at low tide are shown in Figure 11. The flood shoal is exposed, restricting flow from the IWW to travel through the Rockhouse Creek channel. Calculated patterns of wetting and drying of the flood shoal agree with those expected from examination of aerial photographs and shape of the shoal.

Figure 11 shows a well-defined current that extends from the Indian River North and cuts northeast across the inlet, and finally becomes deflected parallel to the north jetty. A region of weak current is present on the south side of the inlet throat, in an area of sediment accumulation. This relatively low-energy area (during this snapshot in time) is present during the turning of the tide. The flood tidal current begins to enter from the south, while the tide is still ebbing in the north throat.

Currents shown in the vector plots (Figures 9 through 11) can assist in identification of scour and depositional processes within Ponce Inlet. Specific problems and hot spots are 1) Scour adjacent to the north jetty along its eastern half, 2) Erosion of the north interior spit, west of the north jetty, and 3) Sediment accumulation within the southern portion of the

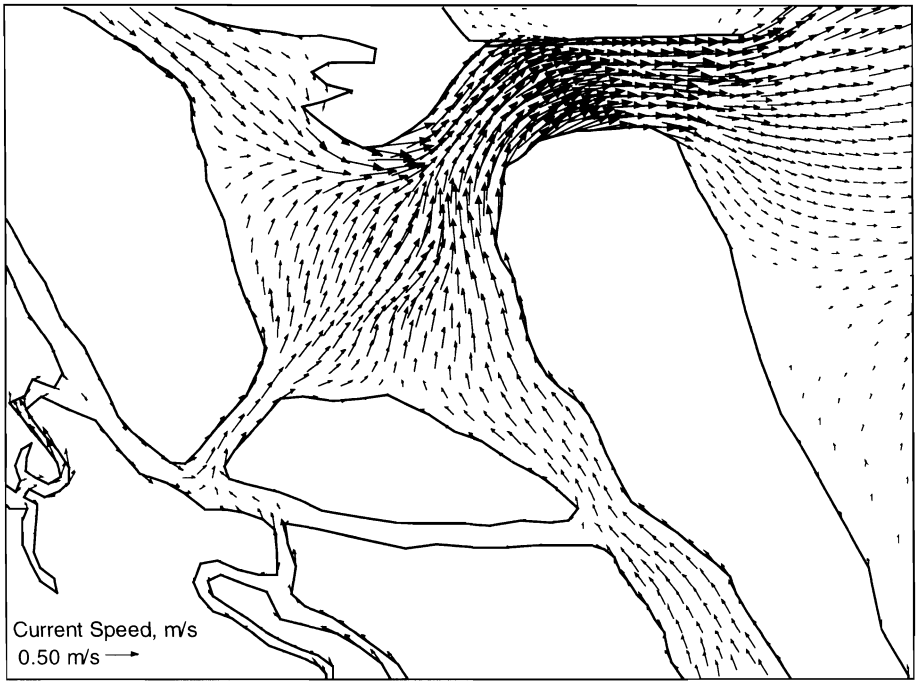

Figure 10. Ebb tide circulation at Ponce Inlet.

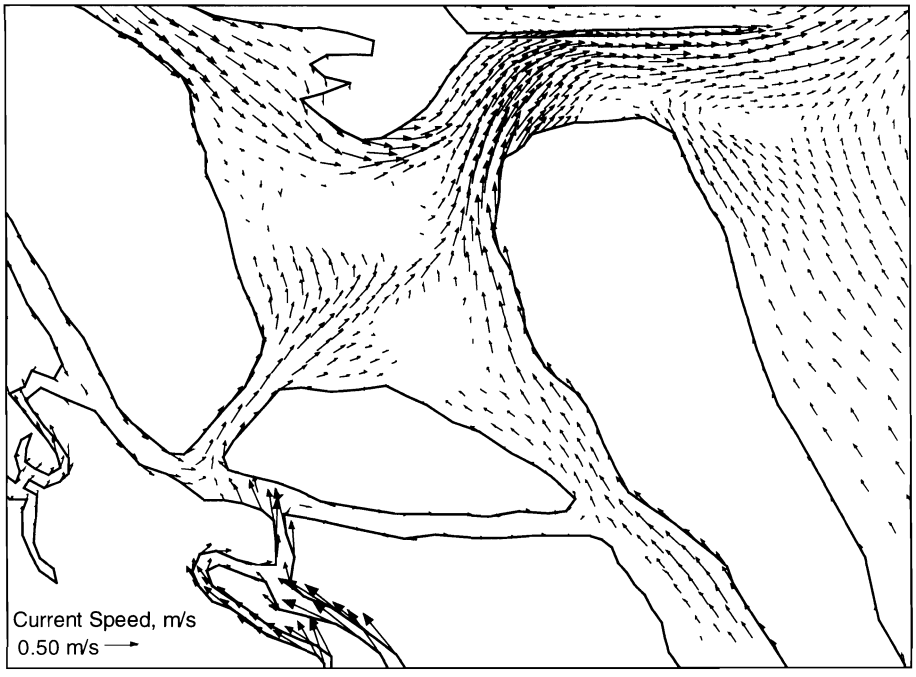

Figure 11. Low tide circulation at Ponce Inlet, tide turning from ebb to flood at entrance.

inlet (prograding south spit). Each of these locations are discussed with reference to associated current patterns.

Scour along the north jetty may be a predominantly ebb-tidal process. Currents within the inlet and adjacent to the north jetty are strongest during ebb tide and are directed parallel to the jetty. During flood tide, the north jetty is a turning point for current flowing in from the north. Curvature of the current keeps the flow from being parallel to the jetty along the eastern jetty end, but the current does become jetty-parallel about one third of the jetty length into the inlet. An additional observation is the northeast-trending current upon ebb flow as it exits the inlet. This flow direction is consistent with the bottom topography, which shows a northeast-trending depression directly east of the north jetty (Figure 5).

During flood tide, the strong current impinges on the north interior spit because of the change in orientation of the inlet. The westward-directed current is deflected toward the southwest as the spit is encountered. Erosion of the spit owes to its being unstructured and being the element that forces curvature of the strong tidal flow.

Accretion of the south spit may occur on both flood and ebb tidal cycles. As shown in Figures 9 and 10, the flow near a portion of the south spit is not directed parallel to the shoreline. Because the spit causes flow curvature as water moves into the inlet (from either the west or the east), a shadow zone may be present where material can be readily deposited. During the turning of the tide, material may accumulate within the southern portion of the inlet as low velocities are present (Figure 11).

The large flood shoal may owe to flood dominance of the system. Accumulation of material at the flood shoal hindered dredging of the IWW when the channel was routed through the shoal. Shoaling of the IWW was sufficient to cause its relocation to the west of the shoal.

TIDAL ATTENUATION

Tidal attenuation in inlet and bay systems depends upon several variables including inlet and bay geometry, presence and extent of tidal flats and shoals, and tidal-constituent frequency (KEULEGAN, 1951; BOON and BYRNE, 1981; AUBREY and SPEER, 1985). Water flowing into the back-bay system at Ponce Inlet must travel north or south through the channelized system before arriving at one of the two primary embayments connected to the inlet. Focus is placed here on the reach extending from the ocean to Station E. This reach was selected for analysis because of the presence of the Coronado Beach bridge between Station E and the ocean, and the better calibration at Station E as compared to Station F.

Tidal attenuation is examined by estimation of the M_2 amplitude along a transect that extends from the ebb shoal to Station E, a distance of 7 km. M_2 amplitudes were estimated from spectral analysis conducted for calculated water-level time series at 14 numerical gauge locations situated along this transect. The dominant energy at all locations is on the M_2 tidal frequency and no significant energy appears on other frequencies. Because motion on tidal frequencies other than the M_2 is absent, nonlinear interactions between the various tidal frequencies are not expected to complicate the analysis of tidal attenuation.

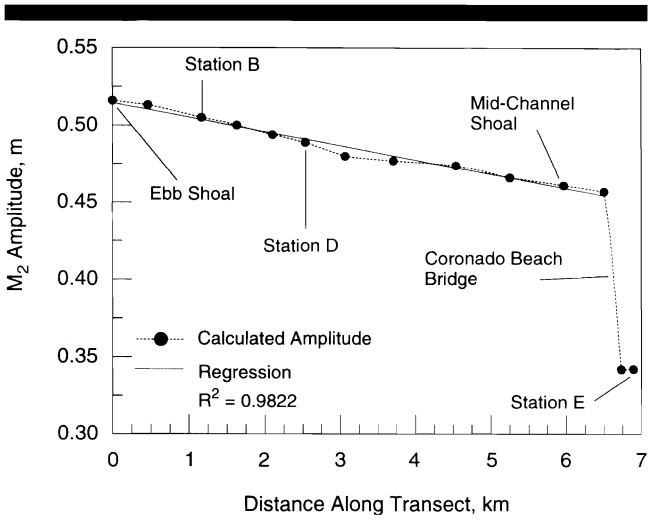

Figure 12. Calculated tidal amplitude at points ranging from the Atlantic Ocean (ebb shoal) to Station E (south of Coronado Beach Bridge).

M_2 amplitudes for the along-channel transect are shown in Figure 12. The point denoted as "Mid-Channel Shoal" is located in the Indian River North, adjacent to the shoal located approximately 1.3 km south of the confluence of the IWW and Indian River North (Figures 4 and 5). The attenuation along the channel is relatively constant over the transect until the Coronado Beach Bridge is reached. A linear regression of tidal amplitude between the ocean and the bridge gave a coefficient of determination (R^2) of 0.9822, indicating a linear attenuation of the tide. At the Coronado Beach Bridge, a significant drop in tidal amplitude occurs, indicating that the bridge behaves as a point source of attenuation.

Tidal attenuation shown in Figure 12 is fairly consistent along the transect until the Coronado Beach bridge is reached. The attenuation of the M_2 tidal amplitude over the ocean-to-bridge reach is 1.1 cm/km. The change in amplitude across the bridge is significant, with the attenuation being approximately 55 cm/km (calculated from the two points in Figure 12 located on each side of the bridge). Comparison of the gradients in amplitude reveal that attenuation under the bridge is 50 times that in the unimpeded channel.

A linear measure of tidal attenuation R is given by

$$R = \frac{A_{Stn}}{A_{Ref}} \tag{1}$$

where A_{Sm} is the tidal amplitude at a specific location internal to the system, and A_{Ref} is the tidal amplitude at a reference station, taken here to be the numerical gauge located on the ebb shoal. In a system where the tidal wave is damped, R can range between zero and one where a value of zero indicates complete damping of the tide and a value of one indicates no damping. Figure 13 shows the attenuation along the transect as parameterized by R. Approximately 5% of the tidal amplitude is attenuated through the inlet, and about 12% is attenuated between the ocean and Coronado Beach

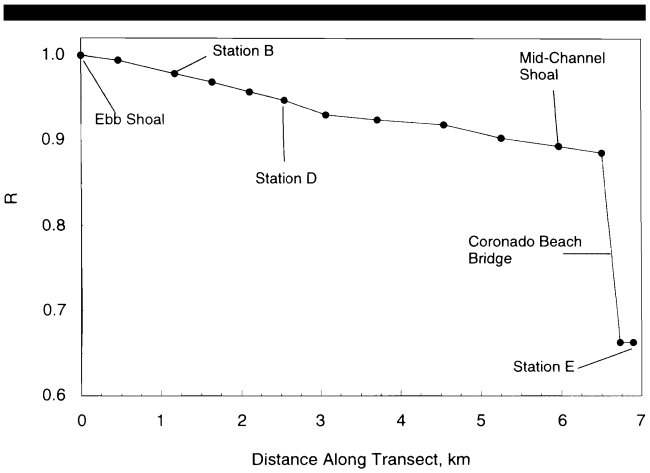

Figure 13. Attenuation of the M_2 tidal constituent at points ranging from the Atlantic Ocean (ebb shoal) to Station E.

Bridge. The bridge reduces the tidal amplitude another 22% from its value at the ebb shoal.

The concept of point-source attenuation of tidal motion at bridges is proposed here, and a simple approximation of tidal-amplitude reduction at the Coronado Beach Bridge is presented. Results from this study can be qualitatively considered with respect to 1) attenuation in systems with multiple bridges, and 2) interpretation of water-level data collected under bridges in tidal flow. In the situation of multiple bridges, successive point attenuation of the tidal signal may occur, resulting in structure-induced reduction in the tidal amplitude that could be significantly greater than the unstructured condition. From a circulation modeling perspective, representation of the bridges is found to be necessary for accurate calculation of the hydrodynamics.

Because the tidal amplitude can vary by several centimeters on either side of a bridge, one must be careful in interpretation of water-level data collected under a bridge. Two cases in point are calibration of a circulation model and estimation of water-surface slope over a channel reach. The gradient in water surface under a bridge can be great relative to a typical reach of channel, and the steep gradient would be limited to the bridge section. Calibration of a circulation model to measurements collected under a bridge could lead to inaccuracies in the solution if the bridge is not represented appropriately. Inaccurate (or no) representation of a bridge could result in artificially high damping of the tidal amplitude between the bridge and inlet. Similarly, if calculating water slope over a reach and water-level measurements were taken under a bridge, calculated surface slope may be greater than the actual slope.

DISCUSSION AND CONCLUSIONS

Measurements of water level and current were successfully collected at Ponce Inlet and in the adjacent bay channels over a 10-week interval from August 1997 through October 1997. Currents within Ponce Inlet peak at approximately 1 m/s and are sufficient to maintain the inlet. The Ponce Inlet system was flood-dominated during the measurement period. Station F in the Halifax River exhibited strong tidal asymmetry, with the duration and magnitude of the flood flow exceeding that of the ebb flow. During the measurement period, the current at Station E was directed upstream.

Stations positioned far from the inlet (5 km) in the Indian River North and Halifax River (Stations E and F, respectively) exhibited a net influx of water over the measurement period. Processes responsible for the influx were not investigated. The influx toward the south was sufficiently strong to eliminate seaward flow during the ebb portion of the tidal cycle at Station E. Tidal asymmetry at Station F and possibly within the inlet may have had increased bias toward flood flow because of the long-period influx of water.

Calculations from the two-dimensional model applied to the site generally agreed with measurements for tidal flow. Average difference between measurements and calculations of water-level amplitude of the M_2 tidal constituent was 5 cm. Calculated patterns of inundation and exposure of the flood shoal were realistic and tidal currents responded to changes in water coverage of the shoal.

Circulation patterns calculated in the inlet appear to be realistic and suggest processes responsible for scour and deposition in local areas. Scour along the eastern north jetty may be predominantly an ebb process as the strong ebb tidal current flows parallel to and adjacent to the jetty. Erosion of the north interior spit (west of the jetty) owes to impinging flood currents. The north interior spit is positioned just west of a change in channel orientation which forces the strong flood current to be redirected at the location of the north interior spit.

Accretion at the south spit may occur on both ebb and flood tidal cycles. Currents on the edge of the spit are relatively weak because of a turning of the current and the preferential location for strongest currents to be in the northern section of the inlet. The spit shoreline lies in a shadow zone where material can be deposited.

Ponce Inlet and the Indian River North exhibit linear tidal-amplitude decay where across-channel structures are not present. Between the ebb shoal and the Coronado Beach Bridge, a representative M_2 amplitude reduction in water level is 1.1 cm/km. The concept of point-source tidal attenuation by the presence of bridges was introduced in this study and quantified at the Coronado Beach Bridge. Attenuation of the M_2 tide was estimated to be 50 times greater under the bridge than in the unimpeded channel. In terms of percent attenuation of water level, the Coronado Beach Bridge was calculated to account for approximately 55% of the M_2 tidal amplitude attenuation between the ocean and the bridge. The fact that hydraulic structures, such as bridges, can damp the tidal signal to such as high degree can be significant in terms of modification of circulation patterns, flushing, and possibly sedimentation patterns in channels. Clearly, point sources of attenuation alter the natural channel or bay circulation, and the presence of these structures must be taken into account for understanding the hydrodynamics of a system.

If bridges are present in a system being modeled, the bridges must be taken into account for realistic simulation of the water level and current. If one calibrates a model to a system

with bridges and neglects the bridges in the calculations, the distribution of flow may not be accurate. Artificially high values of bottom roughness coefficients may be required to damp a tidal signal in an unrestricted channel to the extent that a bridge would modify the signal.

ACKNOWLEDGEMENTS

This paper was prepared under Work Unit 32934 as part of the Coastal Inlets Research Project conducted at the U.S. Army Engineer Waterways Experiment Station. The Jacksonville District of the U.S. Army Corps of Engineers and the Ponce de Leon Inlet Navigation District provided supplemental support for this study. The authors thank Nick Kraus for review of the manuscript. Permission to publish this paper was granted by the Chief of Engineers, U.S. Army Corps of Engineers.

LITERATURE CITED

AUBREY, D.G. and SPEER, P.E., 1985. A Study of Non-linear Tidal Propagation in Shallow Inlet/Estuarine Systems. Part I: Observations. *Estuarine, Coastal and Shelf Science,* 21, 185–205.

BOON, J.D. and BYRNE, R.J., 1981. On Basin Hypsometry and the Morphodynamic Response of Coastal Inlet Systems. *Marine Geology,* 40, 27–48.

BROWN, C.A.; KRAUS, N.C., and MILITELLO, A., 1995. Hydrodynamic Modeling for Assessing Engineering Alternatives for Elevating the Kennedy Causeway, Corpus Christi, Texas. *Proceedings of the 4th International Conference on Estuarine and Coastal Modeling,* (ASCE), pp. 681–694.

HARKINS, G.S.; PUCKETTE, P., and DORRELL, C., 1997. Physical Model Studies of Ponce DeLeon Inlet, Florida. *Technical Report CHL-97-23,* U.S. Army Engineer Waterways Experiment Station, Vicksburg, MS.

HAYES, M.O., 1979. Barrier island morphology as a function of tidal and wave regime. *In: Barrier Islands,* LEATHERMAN, SP.P. (ed.), New York: Academic, 1–27.

JONES, C.P. and MEHTA, A.J., 1978. Ponce De Leon Inlet, Glossary of Inlets Report #6. Florida Sea Grant Program, FL.

KEULEGAN, G.H., 1951. Third Progress Report on Tidal Flow in Entrances: Water Level Fluctuations of Basins in Communication with Seas. *Report No. 1146,* National Bureau of Standards, Washington, D.C.

KING, D.B.; SMITH, J.M.; MILITELLO, A.; STAUBLE, D.S. and WALLER, T.N., 1999. Ponce de Leon Inlet, Florida, Site Investigation. Report 1: Selected Portions of Long-Term Measurements 1995–1997. *Technical Report CHL-99-1,* U.S. Army Engineer Waterways Experiment Station, Vicksburg, MS.

LILLYCROP, W.J.; PARSON, L.E., and IRISH, J.L., 1996. Development and Operation of the SHOALS Airbourne Lidar Hydrographic Survey System. *In: Laser Remote Sensing of Natural Waters: From Theory to Practice,* V.I. FEIGELS, and KOPILEVICH, Y.I. (ed.), Proc., SPIE 2964, pp. 26–37.

LUETTICH, R.A.; WESTERINK, J.J., and SCHEFFNER, N.W., 1992. ADCIRC: An Advanced Three-Dimensional Circulation Model for Shelves, Coasts, and Estuaries, Report 1, Theory and Methodology of ADCIRC-2DDI and ADCIRC-3DL. *Technical Report DRP-92-6,* U.S. Army Engineer Waterways Experiment Station, Vicksburg, MS.

MEHTA, A.J., 1996. A Perspective on Process Related Research Needs for Sandy Inlets. *Journal of Coastal Research,* 23, 3–21.

O'BRIEN, M.P., 1969. Equilibrium Areas of Inlets on Sandy Coasts. *Journal of Waterways, Harbors and Coastal Engineering Division,* (ASCE) 95 (WW1), 43–52.

PARTHENIADES, E. and PURPURA, J.A., 1972. Coastline Changes Neat a Tidal Inlet. *Proceedings of the Thirteenth Coastal Engineering Conference,* (ASCE), pp. 843–863.

PURPURA, J.A., 1977. Performance of a Jetty-Weir Inlet Improvement Plan. *Proceedings of Coastal Sediments 1977* (ASCE), pp. 330–349.

SMITH, J.S. and SMITH, J.M., in press. Numerical Modeling of Waves at Ponce de Leon Inlet, Florida. *Journal of Waterway, Port, Coastal and Ocean Engineering.*

SURAK, C.R., 1994. Forcing at Tidal and Subtidal Frequencies in the Indian River Lagoon, Florida. M.S. Thesis, Division of Marine and Environmental Systems, Florida Institute of Technology, Melbourne, FL.

TAYLOR, R.B.; HULL, T.J.; SRINIVAS, R., and DOMPE, P.E., 1996. Ponce DeLeon Inlet Feasibility Study, Numerical Modeling and Shoaling Analysis, Volume I. Taylor Engineering, Inc., Jacksonville, FL.

WESTERINK, J.J.; LUETTICH, R.A., and SCHEFFNER, N., 1993. ADCIRC: An Advanced Three-Dimensional Circulation Model for Shelves, Coasts, and Estuaries, Report 3, Development of a Tidal Constituent Database for the Western North Atlantic and Gulf of Mexico. *Technical Report DRP-92-6,* U.S. Army Engineer Waterways Experiment Station, Vicksburg, MS.

ZARILLO, G.A. and MILITELLO, A., 1999. Ponce de Leon Inlet, Florida, Site Investigation. Report 2: Inlet Hydrodynamics: Monitoring and Interpretation of Physical Processes. *Technical Report CHL-99-1,* U.S. Army Engineer Waterways Experiment Station, Vicksburg, MS.

ZARILLO, G.A.; WARD, L.G., and HAYES, M.O., 1982. *An Illustrated History of Tidal Inlet Changes in South Carolina.* South Carolina Sea Grant Consortium, 76p.